Two-photon excitation microscopy of tryptophan-containing proteins

M. Lippitz[†], W. Erker[‡], H. Decker[‡], K. E. van Holde[‡§], and T. Basché[†¶]

[†]Institute of Physical Chemistry, Jakob-Welder-Weg 11, and [‡]Institute of Molecular Biophysics, Jakob-Welder-Weg 26, University of Mainz, 55099 Mainz, Germany

Contributed by K. E. van Holde, December 11, 2001

We have examined the feasibility of observing single protein molecules by means of their intrinsic tryptophan emission after two-photon excitation. A respiratory protein from spiders, the 24-meric hemocyanin, containing 148 tryptophans, was studied in its native state under almost *in vivo* conditions. In this specific case, the intensity of the tryptophan emission signals the oxygen load, allowing one to investigate molecular cooperativity. As a system with even higher tryptophan content, we also investigated latex spheres covered with the protein avidin, resulting in 340 tryptophans per sphere. The ratio of the fluorescence quantum efficiency to the bleaching efficiency was found to vary between 2 and 180 after two-photon excitation for tryptophan free in buffer solution, in hemocyanin, and in avidin-coated spheres. In the case of hemocyanin, this ratio leads to about four photons detected before photobleaching. Although this number is quite small, the diffusion of individual protein molecules could be detected by fluorescence correlation spectroscopy. In avidin-coated spheres, the tryptophans exhibit a higher photostability, so that even imaging of single spheres becomes possible. As an unexpected result of the measurements, it was discovered that the population of the oxygenated state of hemocyanin can be changed by means of a one-photon process with the same laser source that monitors this population in a two-photon process.

By eliminating ensemble averaging, single-molecule fluorescence microscopy and spectroscopy (1–4) have proven to obtain novel insights into the dynamics of complex heterogeneous systems (5–7). In the field of biological applications, confocal scanning and wide-field fluorescence microscopy of single protein molecules have been used to study conformational transitions (8–10), enzyme kinetics (11), local pH in cells (12), and diffusion in membranes (13) and cells (14) (for a review see ref. 15). Although the most general single molecule application relies on the use of fluorescent dyes, which are attached to the biomolecule of interest, the intrinsic fluorescence emission of biomolecules has also been utilized in some cases (16–18).

In the present study, we have explored the potential of fluorescence detection of single proteins by making use of the intrinsic tryptophan (Trp) emission. Although aromatic amino acids as Trp or tyrosine are abundant in many biopolymers, to our knowledge there have been no reports on single-molecule detection of Trp or proteins containing Trp. Actually, there are a number of reasons for the lack of reports, mainly relating to the problem of excitation in the UV ($\lambda_{max} = 280$ nm) and the limited photostability of UV-absorbing chromophores like Trp.

Because of the supposedly low photostability of Trp, we have concentrated on systems that contain a large number of Trps. One particular class of material we have investigated are hemocyanins, which are large multisubunit proteins functioning as respiratory proteins in the hemolymph of arthropods and mollusks (19–21). One of the hemocyanins best investigated is the 4×6-meric hemocyanin (Hc) from the tarantula *Eurypelma californicum*. The complete sequences of the subunits for this species are known (22), and the oxygen binding is well understood (23–25). One molecule of oxygen is reversibly bound between two copper atoms in a transverse coordination (26). The oxygen–copper complex gives rise to two ligand-to-metal charge-transfer absorption bands that are centered at 340 nm ($\varepsilon \approx 20{,}000\ M^{-1}\cdot cm^{-1}$ per binding site; ref. 27) and 570 nm ($\varepsilon \approx 1{,}000\ M^{-1}\cdot cm^{-1}$). The short-wavelength absorption band overlaps with the Trp emission band and results in an almost complete quenching of the Trp fluorescence because of Förster transfer (28, 29). Therefore, in Hc the intensity of the Trp fluorescence monitors the oxygen load (25) and can therefore be used for obtaining oxygen binding curves (23, 25) and to clarify the mechanism of the cooperative oxygen binding. Considering the above features, *Euryplema* Hc was identified as an appropriate candidate for our investigations. First, it contains 148 Trp residues (22), and second, the Trp emission intensity monitors the oxygen load. Therefore, experiments at the single protein level promised—besides the envisioned imaging—to allow the study of conformational transitions assumed to occur between different levels of oxygenation of Hc.

To overcome the problem of direct UV excitation of Trp, we have used two-photon excitation (TPE) (30, 31), which was previously applied to single-molecule detection by Mertz *et al.* (32). This technique promises to selectively excite transitions in the UV by visible pulsed laser sources without the broad unspecific background of conventional, one-photon excitation (OPE) in the UV. Compared with fluorescent dyes (33) that were studied in the first two-photon experiments (32), Trp has a rather low two-photon absorption cross section (34). This disadvantage seems to be partly compensated by the large number of Trps in a single Hc. Another important issue is the photostability of Trp after TPE. To get an idea about the photobleaching quantum efficiency of Trp in different environments besides Hc, we also studied unbound Trp and the Trp-containing protein avidin bound to latex spheres.

Materials and Methods

Hc of the tarantula *E. californicum* was purified and tested according to ref. 23. The buffer used was 0.1 M Tris·HCl at pH 7.8 in the presence of 5 mM $CaCl_2$ and 5 mM $MgCl_2$. Trp purchased from Fluka (Neu-Ulm, Germany) was dissolved in the same buffer and used without further purification. For control experiments, Hc was labeled with tetramethylrhodamine (TMR; Molecular Probes). Ten parts Hc solution (2 μM) in borate buffer (25 mM borate/NaOH, pH 8.5/5 mM $CaCl_2$/5 mM $MgCl_2$) was mixed with three parts of dye solution (1 mM) and incubated for 2 h in the dark. The Hc was purified by gel filtration and ultracentrifugation in Tris buffer. Latex spheres (diameter: 40 nm) crosslinked on their surface with the protein avidin (Fluospheres, Molecular Probes) were studied as another model

Abbreviations: Hc, hemocyanin; TMR, tetramethylrhodamine; OPE, one-photon excitation; TPE, two-photon excitation; FCS, fluorescence correlation spectroscopy.

[§]Permanent address: Department of Biochemistry and Biophysics, Oregon State University, Corvallis, OR 97331.

[¶]To whom reprint requests should be addressed. E-mail: thomas.basche@uni-mainz.de.

The publication costs of this article were defrayed in part by page charge payment. This article must therefore be hereby marked "*advertisement*" in accordance with 18 U.S.C. §1734 solely to indicate this fact.

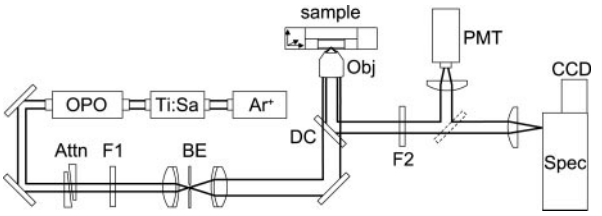

Fig. 1. Diagram of the experimental setup for two-photon microscopy. The laser system consists of an argon-ion-laser (Ar^+), a titanium-sapphire laser (Ti:Sa), and an optical parametrical oscillator (OPO). The light beam is attenuated (Attn), filtered (F1), and expanded (BE) before it is focused by a microscope objective (Obj) onto the sample. The fluorescence light is collected by the same objective, reflected by a dichroic beamsplitter (DC), filtered (F2), and detected by a photomulitplier tube (PMT) or a spectrometer and charge-coupled device camera (CCD).

system. Avidin is a small homotetrameric protein with a molar mass of 66 kg/mol. Each subunit has the ability to bind one molecule of biotin and contains four Trp residues (35). From the biotin-binding capacity given by the manufacturer, the number of Trps per sphere is calculated to be 340. The same avidin-coated spheres with a dye filling have been used for control experiments.

Standard emission spectra were measured in a commercial spectrometer (F-4500, Hitachi, Tokyo) at an excitation wavelength of 295 nm. For TPE at 590 nm (34), Fourier-limited pulses of 180 fs were produced by an optical parametrical oscillator (OPO) with intracavity frequency doubling (Angewandte Physik und Elektronik, Berlin), which was pumped by an argon-ion/titanium-sapphire laser source (Coherent Radiation, Palo Alto, CA; see Fig. 1). The light was focused by a microscope objective (Ultrafluar 100×, numeric aperture = 1.2, Zeiss) onto the sample. The fluorescence emission was collected by the same objective and separated from the excitation light with a custom-made dichroic beam splitter and filter set with a transmission window from 310 to 380 nm (both AHF Analysentechnik, Tübingen, Germany). The fluorescence light was either detected by a Peltier-cooled photomultiplier (R4220P, Hamamatsu, Middlesex, NJ) or analyzed with a monochromator and a liquid N_2-cooled charge-coupled device camera (Roper Scientific, Trenton, NJ). Two-dimensional images were acquired by scanning the sample through the focus. The image acquisition was controlled by a photon counter (SR400, Stanford Research, Sunnyvale, CA) that registers the fluorescence count rate and synchronously moves the scanning stage. For ensemble experiments (at higher concentrations), the fluorescence was collected from a fixed focal volume within the solution. The solution could be stirred and purged with nitrogen or oxygen to control the degree of oxygenation of the Hc. In the experiments described below, we used an oxygen content of 0.7% (5 torr partial pressure; 1 torr = 133 Pa) for the deoxygenated samples. At this condition, almost all Hc molecules are in the deoxygenated state (23, 25). At 20% oxygen content (150 torr partial pressure) in the oxygenated sample, all Hc molecules are fully oxygenated. For fluorescence correlation spectroscopy (FCS), a digital autocorrelator card (ALV 5000/E, ALV, Langen, Germany) was used. Control experiments with TMR-labeled Hc and dye-filled avidin-coated spheres were conducted with a confocal one-photon laser scanning microscope (36).

Results

Intensity Dependence of the Fluorescence Count Rate. After establishing that the fluorescence emission spectra of the Trp residues in Hc after OPE and TPE are identical (excitation wavelength 295 and 590 nm, spectra not shown here), we have investigated the intensity dependence of the fluorescence count rate of Trp

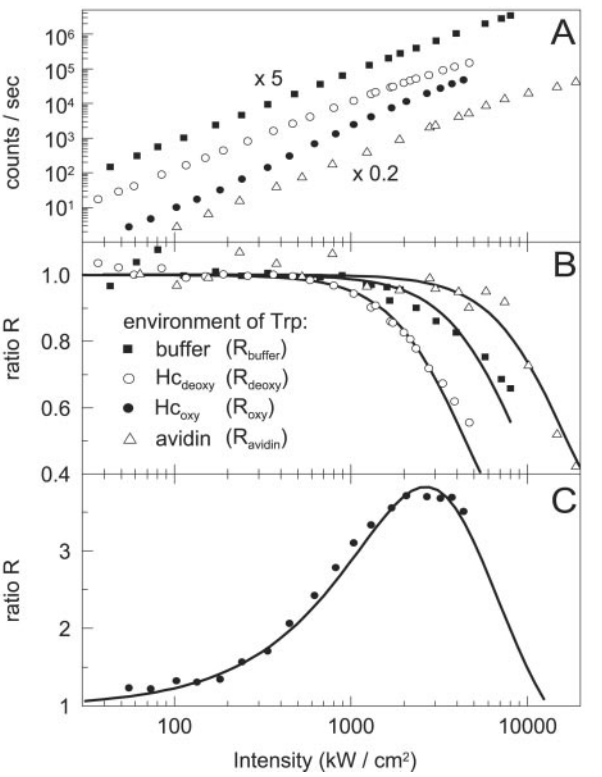

Fig. 2. Excitation intensity dependence of the Trp fluorescence count rate. (*A*) A 1 mM Trp solution (buffer) shifted by a factor of 5 for clarity, a 50 nM solution of avidin-coated spheres (avidin), and 2 μM Hc solutions in the oxygenated (Hc_{oxy}) and deoxygenated state (Hc_{deoxy}). Background fluorescence is subtracted. (*B* and *C*) Ratios of the measured to the expected fluorescence count rate. The data are fitted with models discussed in the text.

in Hc and compared it to Trp in buffer solution and in avidin-coated spheres. Fig. 2*A* shows the intensity dependence of the fluorescence count rate after TPE for four different samples: a 1 mM Trp solution, a 50 nM solution of avidin-coated spheres and two 2 μM solutions of Hc in the oxygenated (Hc_{oxy}) and the deoxygenated state (Hc_{deoxy}). The background fluorescence of a blank solution is subtracted from all curves. In a first approximation, a quadratic intensity dependence of the fluorescence count rate would be expected for all four samples when excited by a two-photon process. In Fig. 2 *B* and *C* we have plotted the ratio R between the measured (background-corrected) fluorescence signal F_{exp} and $F_0 = \beta I^2$, which is a measure of the expected fluorescence signal. β is eliminated by normalizing R to unity at the low intensity plateau. Any deviation of this ratio from unity signals a behavior that is not in accordance with a simple quadratic intensity dependence of the fluorescence signal. Along these lines the drop of R below unity in Fig. 2*B* indicates a fluorescence signal that is weaker than expected. This deviation can be explained by photobleaching. On the other hand, the relative fluorescence increase in the case of Hc_{oxy} in Fig. 2*C* is attributed to the intensity-dependent buildup of a state with higher fluorescence efficiency (see *Fluorescence Increase of Oxygenated Sample*).

FCS of Hc. In FCS, diffusion of individual fluorescent molecules can be followed by analyzing the fluctuations of the fluorescence count rate F when the molecules enter or leave the detection volume. The fluctuations of F are described in terms of the normalized autocorrelation function $G(\tau)$ defined as (37)

$$G(\tau) = \frac{\langle \delta F(t) \delta F(t+\tau) \rangle}{\langle F(t) \rangle^2}, \qquad [1]$$

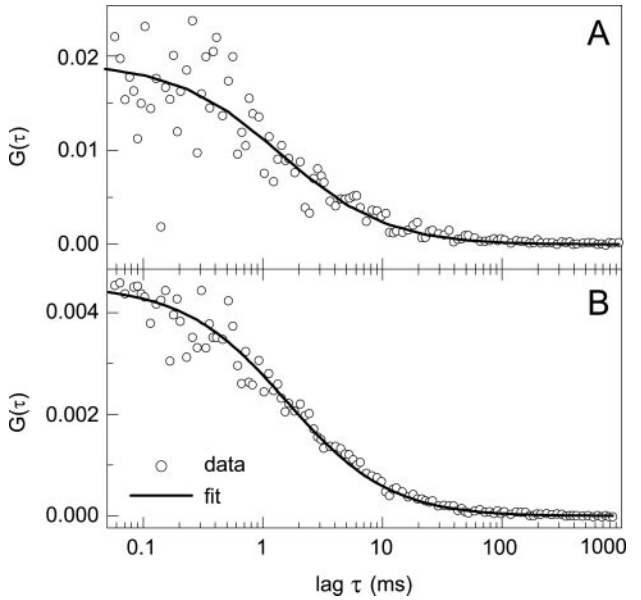

Fig. 3. Fluorescence correlation functions of Hc solutions. (*A*) Intrinsic Trp fluorescence of Hc_{deoxy} after TPE. (*B*) Hc labeled with TMR, measured in a confocal microscope with OPE. Both traces are fitted with models discussed in the text.

where the angular brackets denote the time average and $\delta F(t) = F(t) - \langle F(t)\rangle$ describes the fluctuation of F. The experimental setup used defines a detection volume from which the fluorescence originates. This detection volume is described by the molecule detection efficiency function MDE(**r**). For OPE in a confocal microscope, Rigler *et al.* (38) have shown that MDE(**r**) can be approximated by a three-dimensional Gaussian with $1/e^2$ radii ω_0 (perpendicular to beam direction) and z_0 (along beam direction).

With the effective volume V_{eff} defined as

$$V_{\text{eff}} = \int \text{MDE}(\mathbf{r})dV = \sqrt{\pi^3/8}\omega_0^2 z_0, \qquad [2]$$

a volume contrast factor $\gamma \approx 0.35$ and an average concentration $\langle C\rangle$ the correlation function of free diffusion $G(\tau)$ reads (14, 37)

$$G(\tau) = \frac{\gamma}{V_{\text{eff}}\langle C\rangle}\left(1 + \frac{4D\tau}{\omega_0^2}\right)^{-1}\left(1 + \frac{4D\tau}{z_0^2}\right)^{-1/2}. \qquad [3]$$

In the case of TPE, the approximation of MDE(**r**) by a three-dimensional Gaussian leads to inconsistent absolute values of focal size ω_0, concentration $\langle C\rangle$ and diffusion coefficient D when compared with values measured independently by different experimental techniques (14, 39). Therefore, in the TPE experiments, we have to use the computationally more demanding autocorrelation function given by Berland *et al.* (39), which correctly reproduces all three parameters. This autocorrelation function is based on a squared Gaussian–Lorentzian detection efficiency function MDE(**r**). This shape of the focus leads to an effective volume of $V_{\text{eff}} = \pi^3\omega_0^4/4\lambda$, where λ is the excitation wavelength.

Fig. 3*A* shows the autocorrelation trace of a 20 nM deoxygenated Hc solution after TPE of the Trp residues. The $1/e^2$ radius ω_0 of the laser focus is independently measured as 430 nm (the back aperture of the microscope objective is underfilled). Under these conditions, only four molecules are on average simultaneously diffusing through the effective focal volume of 0.46 fl. The data are the result of 30-min integration time and an excitation intensity of 2 MW/cm^2, which yields an average count rate of 1,200 cps. By fitting the autocorrelation function of ref. 39 to the data, we obtain a diffusion coefficient D of 1.9×10^{-7} cm^2/s and a concentration of 8 molecules per focal volume. The relative error is in the order of 10%. The number of molecules obtained from the fit overestimates the actual value by a factor of 2. This overestimation is caused by the background fluorescence (37). About 10% of the count rate is caused by fluorescence of the buffer and can be detected in a blank sample. Another contribution is from Hc molecules, which produce only one count, either because they photobleach or because the excitation intensity is too low to produce more counts. This single count is not correlated to any other counts so that it appears as a background count.

In a control experiment we have measured the fluorescence correlation function of TMR-labeled Hc after OPE at 488 nm in a confocal microscope. Each protein was labeled by about 3 dye molecules. The resulting correlation function is shown in Fig. 3*B*. In this case the protein concentration, the mean count rate, and the integration time were 200 nM, 11 kcps, and 25 min, respectively. Fitting Eq. **3** to the data gives a diffusion coefficient $D = 2.1 \times 10^{-7}$ cm^2/s, which within the measurement uncertainty is the same value as obtained from TPE.

Imaging of Proteins. Imaging of single particles has to date been successful only for avidin-coated spheres. The spheres were adsorbed at low coverage on a glass coverslip and imaged by means of the Trp emission after TPE. A typical example of such an image is shown in Fig. 4*A*. In some of the bright spots up to 30 counts per pixel are detected. The background of a blank sample is in the range of 2–3 counts per pixel. None of the bright spots assumes a fully circular shape, most probably because of photobleaching during image acquisition. Occasionally single horizontal lines along the scan direction are observed, which may result from spheres drifting through the focus. Fig. 4*B* shows two horizontal linescans at the positions indicated in Fig. 4*A*, which give an impression of the signal-to-noise ratio obtained.

The same kind of avidin-coated spheres is available filled with fluorescent dye. We imaged these dye-filled spheres in a confocal microscope (OPE) to check the adsorption and coverage of the spheres on a coverslip under buffer solution. The number of spheres observed on the surface is comparable in the OPE and TPE experiments when the preparation conditions of the samples are similar. This finding excludes the possibility that the bright spots in the two-photon image (Fig. 4*A*) are only large aggregates of avidin-coated spheres.

Discussion

Photobleaching. Many experiments relying on sensitive fluorescence detection are severely hindered by photobleaching of the fluorophores because it limits the signal to noise ratio available. This detrimental effect is especially important for UV-absorbing fluorophores. In the following paragraphs we will give an estimation of the photobleaching quantum efficiency of Trp in different environments, based on a method proposed recently by Mertz (40). The photobleaching quantum efficiency q_b phenomenologically describes the probability for an excited fluorophore to bleach. The bleaching reduces the number of (active) fluorophores in the focal volume and therefore reduces the fluorescence count rate. In the present context R, which was introduced before, reads as the ratio between the fluorescence count rate in the presence of photobleaching (F_{exp}) to that of an ideal sample without bleaching (F_0), which, according to ref. 40, can be expressed as:

$$R = \frac{F_{\text{exp}}}{F_0} = \frac{1}{1 + \alpha\gamma q_b \tau_d}, \qquad [4]$$

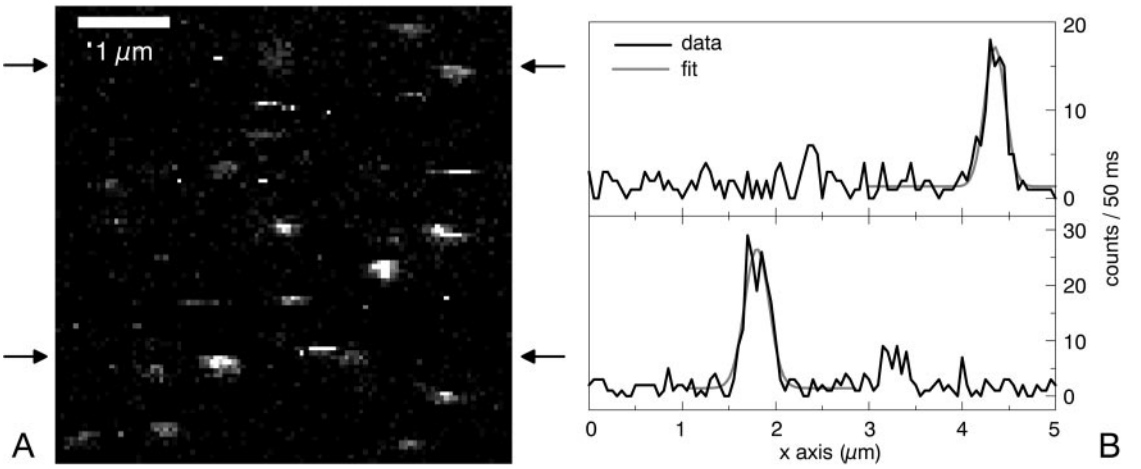

Fig. 4. (*A*) TPE fluorescence image of avidin proteins bound to latex spheres, each containing 340 Trp molecules ($I = 750$ kW/cm^2 at 590 nm; integration time per pixel: 50 ms; image size: 5×5 μm). (*B*) Horizontal linescans at the positions indicated in *A*. Fitting the data to a Gaussian yields a focal spot size of $\omega_0 = 350$ nm.

where α is the excitation rate of a molecule in the center of the focus and τ_d is the average dwell time between the first entry and the last exit of a molecule in the detection volume. For a Gaussian–Lorentzian focus in the case of TPE (volume contrast factor $\gamma = 3/16$) τ_d can be approximated by (40):

$$\tau_d \approx \frac{\omega_0^2}{1.8\,D} \ln\left(6\frac{\pi\omega_0}{\lambda}\right) \qquad [5]$$

with $\omega_0 = 350$ nm and $\lambda = 590$ nm. The excitation rate α of one Trp residue in the center of the focus can be calculated as (41):

$$\alpha = \tfrac{1}{2}\,\sigma\,\frac{0.66}{f\tau}\left(\frac{I}{h\nu}\right)^2, \qquad [6]$$

where $\sigma \approx 1 \times 10^{-50}$ cm^4·s (34) is the two-photon absorption cross section, $f = 76$ MHz the repetition rate and $\tau = 180$ fs the pulse width of the laser. We assume equal absorption cross sections σ for Trp in all environments investigated.

Putting together Eqs. **4**, **5**, and **6**, R is fitted to the data in Fig. 2*B*. Depending on the sample studied, R is denoted as R_{buffer}, R_{deoxy}, or R_{avidin}.

The data slightly deviate from the model, which may be the result of an intensity dependence of q_b. This intensity dependence could be caused by an additional two-step photobleaching process (40, 42) in which the molecule bleaches by absorption of a third photon in contrast to the case of constant q_b, where the bleaching process is assumed to involve no further absorption of photons.

The results of the fitting procedure are summarized in Table 1. It is clearly seen that the photobleaching quantum efficiency q_b is highest for Trp dissolved in buffer solution. With a fluorescence quantum efficiency η of 13% (43) this results in an average of 2 emitted photons per Trp before photobleaching.

Table 1. Photobleaching quantum efficiency q_b and fluorescence quantum efficiency η of Trp in different environments

Environment	D, cm^2·s^{-1}*	τ_d, ms	q_b, %	η, %
Buffer	80×10^{-7}	0.2	6.5	13
Hc_{deoxy}	2×10^{-7}	8	1.5	7
Avidin	1.1×10^{-7}	15	0.07	13

*As an estimate for the diffusion coefficients D for Trp and avidin-coated spheres we used the values for coumarin (47) and uncovered latex spheres (39), respectively.

Taking into account the detection efficiency of our setup (0.6%), the probability of detecting a fluorescence photon before bleaching of the Trp molecule is ≈1%. Under these circumstances, fluorescence detection of single Trp molecules becomes highly improbable.

The photostability of Trp clearly increases in the protein environments. For Trp in Hc_{deoxy} a photobleaching quantum efficiency q_b of 1.5% has been determined from the fit. Compared with a fluorescence quantum efficiency η of 7% for Trp in deoxygenated Hc (29) this number gives an average emission of about 5 photons per Trp before bleaching. Given the Trp content of Hc (148 residues) and the detection efficiency, one deoxygenated Hc molecule produces on average 4 to 5 counts before photobleaching.

The lowest photobleaching quantum yield has been found for Trp in avidin-coated spheres. From the fluorescence quantum efficiency η of 13% (35) it follows that about 180 photons per Trp residue are emitted before bleaching. With 340 Trp residues bound to one latex sphere, the detector should acquire 380 counts per sphere. This estimate coincides with the count rates in Fig. 4.

It should be noted that the calculated photobleaching quantum efficiency q_b varies from sample to sample, so we estimate the relative error to about 30%. Another source of error could be environment-dependent differences in TPE absorption cross section σ of Trp. Because of the lack of experimental data, the TPE absorption cross section had to be assumed to be constant.

Single-Molecule Experiments. The experiments described above have clearly shown that the high photobleaching efficiency will prevent the detection of single Trp molecules. The situation improves for a single Hc_{deoxy} molecule, which contains 148 Trp residues and on average produces 4 counts on the photodetector before bleaching. These 4 counts are not distributed randomly, but all appear during the short transit time of the molecule through the focus—they are correlated to each other. If the background count rate is low enough, the statistical method of FCS finds this correlation in the temporal distribution of the detected photons. As shown in Fig. 3*A*, the number of photons emitted from each Hc_{deoxy} is sufficient to detect the diffusion of a small number of Hc_{deoxy} molecules by FCS after TPE. A fit to the FCS data based on an appropriate model yielded a diffusion coefficient of $D = 1.9 \times 10^{-7}$ cm^2/s. The same diffusion coefficient as in this TPE experiment was found in a conventional OPE setup with TMR-labeled Hc (Fig. 3*B*). The diffusion coefficient can also be calculated from the sedimentation coef-

ficient s. The Svedberg equation (44) can be solved for the diffusion coefficient D,

$$D = \frac{sRT}{M(1 - V\rho)}, \qquad [7]$$

where R is the gas constant and T the absolute temperature. The sedimentation coefficient s, the molecular mass M, the specific molecular volume V, and the density ρ of the solvent have the values 37×10^{-13} s (45), 1,720 kg/mol (22), 0.74 cm^3/g (44), and 1 g/cm^3, respectively. When these values are used, D is calculated to be 2.0×10^{-7} cm^2/s in almost exact agreement with the value measured in this work. This finding underlines that in both experiments we watch the diffusion of individual Hc_{deoxy} molecules and not of molecular aggregates.

For many applications, reproducible two-dimensional imaging of a distribution of single molecules would be desirable. Such an experiment requires several detected photons in several adjacent pixels of the image to distinguish molecules from background. An average of 4 detected photons, as was observed for a single Hc_{deoxy}, is not sufficient for this purpose. Therefore, the photobleaching quantum yield of Trp in deoxygenated Hc while still allowing the detection of single Hcs by FCS, prevents the more demanding imaging of single Hcs by confocal microscopy, at least under present instrumentation limits.

The photostability of Trp was highest in avidin-coated spheres. Again, each latex sphere was covered with about 21 avidin molecules so that each particle in total contains 340 Trp residues. Actually, this is only 2.3 times the Trp content of our Hc, but obviously the increased photostability and quantum efficiency in this environment allows imaging the spheres in our two-photon laser scanning microscope (Fig. 4). This example demonstrates that under favorable conditions the intrinsic fluorescence of Trp residues of proteins may allow the acquisition of fluorescence images of single macromolecules without the introduction of an artificial dye.

Fluorescence Increase of Oxygenated Sample. Although for Trp in Hc_{deoxy} (as well as for Trp in buffer solution and in avidin-coated spheres) R dropped below unity with increasing excitation intensities because of photobleaching, for Trp in Hc_{oxy} the opposite was observed (Fig. 2*C*). To explain the apparent increase in fluorescence intensity, we will refer to a simple model that involves the following equilibria between different states of a single Hc binding site:

$$O_x^* \underset{k}{\overset{k_4}{\rightleftharpoons}} O_x \underset{k_{on}}{\overset{k_{off}}{\rightleftharpoons}} D_x + O_2. \qquad [8]$$

In the absence of light irradiation, the rates k_{on} and k_{off} define the equilibrium population between the oxygenated state O_x and the deoxygenated state D_x of a single binding site. Cooperative interactions between the 24 subunits of a Hc molecule will modify this equilibrium. In the state O_x, a dicopper binding site is loaded by oxygen, which creates two ligand-to-metal charge transfer transitions. Because the transition around 340 nm quenches the Trp fluorescence in the subunit by means of Förster transfer, the Trp fluorescence monitors the population of the O_x state. The second transition gives rise to a comparatively weak and broad absorption band that peaks around 570 nm. The 590-nm pulses used for the TPE of Trp are absorbed in a one-photon process by this transition, generating an excited state O_x^* of one binding site. According to the model, this state does not quench the Trp fluorescence. The population rate k for its formation is proportional to the light intensity at 590 nm. Therefore, besides D_x, O_x^* is fluorescent, too, and higher illumination intensities should increase the population of this state.

By solving the appropriate system of differential equations the relative population Θ of O_x in the steady state and in the limit of complete oxygenation ($[O_2] \to \infty$) is found to be

$$\Theta = \frac{[O_x]}{[O_x] + [O_x^*] + [D_x]} = \left(1 + \frac{k}{k_4}\right)^{-1} = (1 + \kappa I)^{-1}, \qquad [9]$$

with $k/k_4 = \kappa I$. From this it follows that the oxygenated solution in the presence of 590-nm light is not completely in the state O_x (i.e., $\Theta < 1$), and this does not as effectively quench the fluorescence.

As seen in Fig. 2*C*, at low intensities R_{oxy} is close to unity because most subunits are in state O_x and the count rate follows the quadratic intensity dependence. Because each subunit that is in the state O_x^* (or D_x) emits on average 13 times more photons than a subunit in the state O_x (28), a decrease of the population of O_x increases the fluorescence intensity. Photobleaching is taken into account by assuming that the oxygenated sample is affected by the same amount of bleaching as the deoxygenated one, so that bleaching is described by R_{deoxy} as given above. Taken all this together, R_{oxy} can be calculated to

$$R_{oxy} = [\Theta \times 1 + (1 - \Theta) \times 13] \times R_{deoxy}. \qquad [10]$$

The data of Hc_{oxy} in Fig. 2*C* are well fitted by this equation, using κ as a single fit parameter. Using the photobleaching quantum efficiency q_b as an additional fit parameter does not increase the quality of the fit and leads to a bleaching efficiency that is about 40% higher than that in the deoxygenated case. Therefore the assumption made above is justified. The deviation from quadratic excitation intensity dependence of the count rate in the oxygenated case is explained by our simple model with the light-driven population of an excited state O_x^*.

At present it cannot be decided whether the state O_x^* relaxes to O_x by means of oxygen release and subsequent rebinding, as has been suggested recently (46). A more detailed examination of the photophysics of Hc and the question whether oxygen is released by a light-driven process is called for.

Summary. Trp is a fluorescent aromatic amino acid that is abundant in many proteins. Because the addition of dye tags may produce unknown conformational effects, it is therefore important to explore the potential of this native fluorophore for optical single-molecule detection. Because Trp absorbs in the UV spectral region we have excited the chromophore by a two-photon absorption process. To get a more quantitative idea about the supposedly low photostability of Trp, we have compared the photobleaching quantum efficiency of Trp after TPE of three samples: unbound Trp in solution, Trp in Hc_{deoxy}, and Trp in avidin bound to latex spheres. Careful examination of the fluorescence spectra (not presented here) shows that in each case we measure emission from the same states with one- and two-photon excitation. In the case of unbound Trp in aqueous buffer solution, the photobleaching quantum efficiency is highest. This result implies that TPE fluorescence imaging of single Trps will be extremely hard, if not impossible, to achieve. The photobleaching quantum efficiency of Trp decreases appreciably in the protein environments and is lowest in avidin-coated spheres. Because the number of Trps is large in the two systems studied (Hc: 148; avidin-coated spheres: 340) experiments at the single-particle level become feasible. From a single Hc molecule in its deoxygenated state on average 4 photons are detected before photobleaching, whereas this number increases to 380 for avidin-coated spheres. The different photostabilities in the two protein environments define the type of experiment that can be conducted at the single molecule level. In the case of Hc_{deoxy} the diffusion of single proteins could be measured by fluorescence correlation spectroscopy. Because of the higher photostability,

avidin-coated spheres could be successfully imaged by means of TPE in a confocal laser scanning microscope. These results suggest that under favorable conditions Trp-containing biomolecules can be investigated at the single-molecule level without introducing artificial dye labels.

With regard to Hcs, experiments based on monitoring the Trp emission are especially appealing because the intensity of the fluorescence signal reports on the oxygen load. Investigations at the single-molecule level are expected to yield insights into oxygenation distributions and conformational transitions, which, according to existing theories, occur between different levels of oxygenation of Hc. A substantial drawback certainly relates to the quenching of Trp emission in Hc_{oxy} by bound oxygen, because the weak signal of Hc_{deoxy} is further diminished. However, the present study has surprisingly shown that even for ensemble studies, the TPE experiment presents certain advantages. In the case of oxygenated Hc the intensity-dependent apparent increase of the quantum yield tentatively has been explained by a simple three-state model taking into account the linear excitation of the copper–oxygen complex. Therefore, we used the same laser source to populate an excited state by means of linear absorption and probe the ground state by means of quenching of the TPE fluorescence of the Trp. This intrinsic advantage offers exciting perspectives for the study of oxygen release and rebinding in Hcs after photo-excitation.

We acknowledge support by the Deutsche Forschungsgemeinschaft and a Humboldt prize (to K.E.v.H.).

1. Nguyen, C., Keller, R., Jett, J. H. & Martin, J. C. (1987) *Anal. Chem.* **59,** 2158–2161.
2. Mets, Ü. & Rigler, R. (1994) *J. Fluoresc.* **4,** 259–264.
3. Nie, S. M., Chiu, D. T. & Zare, R. N. (1994) *Science* **266,** 1018–1021.
4. Basché, T., Moerner, W. E., Orrit, M. & Wild, U. P., eds. (1997) *Single-Molecule Optical Detection, Imaging and Spectroscopy* (VCH, Weinheim, Germany).
5. Deniz, A. A., Dahan, M., Grunwell, J. R., Ha, T. J., Faulhaber, A. E., Chemla, D. S., Weiss, S. & Schultz, P. G. (1999) *Proc. Natl. Acad. Sci. USA* **96,** 3670–3675.
6. Neuhauser, R. G., Shimizu, K. T., Woo, W. K., Empedocles, S. A. & Bawendi, M. G. (2000) *Phys. Rev. Lett.* **85,** 3301–3304.
7. Yu, J., Hu, D. H. & Barbara, P. F. (2000) *Science* **289,** 1327–1330.
8. Wennmalm, S., Edman, L. & Rigler, R. (1997) *Proc. Natl. Acad. Sci. USA* **94,** 10641–10646.
9. Eggeling, C., Fries, J. R., Brand, L., Gunther, R. & Seidel, C. A. M. (1998) *Proc. Natl. Acad. Sci. USA* **95,** 1556–1561.
10. Ha, T. J., Ting, A. Y., Liang, J., Caldwell, W. B., Deniz, A. A., Chemla, D. S., Schultz, P. G. & Weiss, S. (1999) *Proc. Natl. Acad. Sci. USA* **96,** 893–898.
11. Lu, H. P., Xun, L. Y. & Xie, X. S. (1998) *Science* **282,** 1877–1882.
12. Haupts, U., Maiti, S., Schwille, P. & Webb, W. W. (1998) *Proc. Natl. Acad. Sci. USA* **95,** 13573–13578.
13. Sonnleitner, M., Schutz, G. J. & Schmidt, T. (1999) *Chem. Phys. Lett.* **300,** 221–226.
14. Schwille, P., Haupts, U., Maiti, S. & Webb, W. W. (1999) *Biophys. J.* **77,** 2251–2265.
15. Weiss, S. (1999) *Science* **283,** 1676–1683.
16. Peck, K., Stryer, L., Glazer, A. N. & Mathies, R. A. (1989) *Proc. Natl. Acad. Sci. USA* **86,** 4087–4091.
17. Dickson, R. M., Cubitt, A. B., Tsien, R. Y. & Moerner, W. E. (1997) *Nature (London)* **388,** 355–358.
18. Wennmalm, S., Blom, H., Wallerman, L. & Rigler, R. (2001) *Biol. Chem.* **382,** 393–397.
19. van Holde, K. E. & Miller, K. (1995) *Adv. Protein Chem.* **47,** 1–81.
20. Salvato, B. & Beltramini, M. (1990) *Life Chem. Rep.* **8,** 1–47.
21. van Holde, K. E., Miller, K. I. & Decker, H. (2001) *J. Biol. Chem.* **276,** 15563–15566.
22. Voit, R., Feldmaier-Fuchs, G., Schweikardt, T., Decker, H. & Burmester, T. (2000) *J. Biol. Chem.* **275,** 39339–39344.
23. Decker, H. & Sterner, R. (1990) *J. Mol. Biol.* **211,** 281–293.
24. Robert, C., Decker, H., Richey, B., Gill, S. J. & Wyman, J. (1987) *Proc. Natl. Acad. Sci. USA* **84,** 1891–1895.
25. Loewe, R. (1978) *J. Comp. Physiol. B* **128,** 161–168.
26. Magnus, K. A., Hazes, B., Ton-That, H., Bonaventura, C. & Bonaventura, J. (1994) *Proteins* **19,** 302–309.
27. Solomon, E. I., Tuczek, F., Root, D. E. & Brown, C. A. (1994) *Chem. Rev.* **94,** 827–856.
28. Erker, W., Hübler, R. & Decker, H. (2001) *Protein Sci.* **10,** Suppl. 1, 144.
29. Boteva, R., Ricchelli, F., Sartor, G. & Decker, H. (1993) *J. Photobiol. Photochem. B.* **17,** 145–153.
30. Göppert-Mayer, M. (1931) *Ann. Phys.* **9,** 273–295.
31. Denk, W., Strickler, J. H. & Webb, W. W. (1990) *Science* **248,** 73–76.
32. Mertz, J., Xu, C. & Webb, W. W. (1995) *Opt. Lett.* **20,** 2532–2534.
33. Xu, C. & Webb, W. W. (1996) *J. Opt. Soc. Am. B* **13,** 481–491.
34. Rehms, A. & Callis, P. (1993) *Chem. Phys. Lett.* **208,** 276–282.
35. Kurzban, G. P., Gitlin, G., Bayer, E. A., Wilchek, M. & Horowitz, P. M. (1989) *Biochemistry* **28,** 8537–8542.
36. Kulzer, F., Koberling, F., Christ, T., Mews, A. & Basché, T. (1999) *Chem. Phys.* **247,** 23–34.
37. Thompson, N. L. (1991) in *Topics in Fluorescence Spectroscopy: Techniques*, ed. Lakowicz, J. (Plenum, New York), Vol. 1, pp. 337–378.
38. Rigler, R., Mets, Ü., Widengren, J. & Kask, P. (1993) *Eur. Biophys. J.* **22,** 169–175.
39. Berland, K. M., So, P. T. C. & Gratton, E. (1995) *Biophys. J.* **68,** 694–701.
40. Mertz, J. (1998) *Eur. Phys. J. D* **3,** 55–66.
41. Xu, C. & Webb, W. W. (1997) in *Nonlinear And Two-Photon Induced Fluorescence,* Topics in Fluorescence Spectroscopy, ed. Lakowicz, J. (Plenum, New York), Vol. 5, pp. 471–540.
42. Eggeling, C., Widengren, J., Rigler, R. & Seidel, C. A. M. (1998) *Anal. Chem.* **70,** 2651–2659.
43. Chen, R. F. (1967) *Anal. Lett.* **1,** 35–42.
44. Cantor, C. R. & Schimmel, P. R. (1980) *Biophysical Chemsitry, Part 2: Techniques for the Study of Biological Structure and Function* (Freeman, San Francisco).
45. Schneider, H. J., Markl, J., Schartau, W. & Linzen, B. (1977) *Hoppe Seylers Z. Physiol. Chem.* **358,** 1133–1141.
46. Floyd, J. S., Haralampus-Grynaviski, N., Ye, T., Zheng, B., Simon, J. D. & Edington, M. D. (2001) *J. Phys. Chem. B* **105,** 1478–1483.
47. Brand, L., Eggeling, C., Zander, C., Drexhage, K. H. & Seidel, C. A. M. (1997) *J. Phys. Chem. A* **101,** 4313–4321.